Fluoride-substituted $Li_{6.4}La_3Zr_{1.4}Ta_{0.6}O_{12}$ with Delocalized Electron-Share Accelerates Li^+ Desolvation Kinetics for High-voltage Lithium Metal Batteries

Peng Chen[a], Bing Ding[a,b,c], Hui Dou[a,b,c*], and Xiaogang Zhang[a,b,c]

[a]*Jiangsu Key Laboratory of Electrochemical Energy Storage Technologies, College of Materials Science and Technology, Nanjing University of Aeronautics and Astronautics, Nanjing 210016, P. R. China*

[b]*Shenzhen Research Institute, Nanjing University of Aeronautics and Astronautics, Shenzhen 518000, China*

[c]*National Key Laboratory of Mechanics and Control for Aerospace Structures, Institute for Frontier Science, Nanjing University of Aeronautics and Astronautics, Nanjing 210016, P.R. China*

**Corresponding author.*

E-mail address: dh_msc@nuaa.edu.cn (Hui Dou); azhangxg@nuaa.edu.cn (Xiaogang Zhang)

1. Methods

1.1 Materials and cell assembly

$Li_{6.4}La_3Zr_{1.4}Ta_{0.6}O_{12}$ (LLZTO), NH_4F, $LiCoO_2$ (LCO) and 1M $LiPF_6$ in EC:DEC were purchased from Canrd Technology Co.LtdCanrd. All were dried at 70 °C under vacuum for 24 h to remove moisture. N,N-dimethyl-Formamide (DMF, ≥99%) was bought from Macklin.

1.2 Preparation process of $LLZTO_xF_y$

For low temperature fluorination, LLZTO and NH_4F with mass ratios of 1:0.1, 1:0.2, 1:0.5 were placed separately in a ceramic boat on the down-stream and up-stream in the tube furnace under N_2 atmosphere, respectively. Then, they were

pyrolyzed at 320 °C for 0.5 h with a heating rate of 2 °C min^{-1}. After naturally cooling down to room temperature, the $LLZTO_{0.95}F_{0.05}$, $LLZTO_{0.91}F_{0.09}$ and $LLZTO_{0.71}F_{0.29}$ were obtained.

1.3 Synthesis of $LLZTO_xF_y$@PP separators

The $LLZTO_xF_y$ modified separator was prepared by a simple surface coating method, 90 wt% of $LLZTO_xF_y$ and 10 wt% of PVDF were mixed together in NMP solvent under vigorous stirring to form a homogeneous slurry, which was then coated on pristine Celgard 2500 (PP) separator. The obtained functionalized separator was dried at 60 °C overnight under vacuum. Eventually, the coated separator was cut into discs with a diameter of 19 mm. The optimized coating thickness was 19±5 μm with a areal mass loading of ~ 0.3 mg cm^{-2} (Figure S16).

1.4 Preparation of LCO cathode

90 wt% LCO, 5 wt% Super P, 5 wt% PVDF/NMP (30 mg mL^{-1}) were mixed for 24 h. The resulting mixture was then scraped onto carbon coated Al foil. Subsequently, the cathode was air drying for 6 h and then vacuum dried at 110 °C for 12 h to remove residual NMP. The mass loading of LCO cathode is ~8.0 mg cm^{-2}. While the ~ 2.0 mg cm^{-2} for cyclic voltammetry (CV) test.

1.5 Battery assembly

The assembly of the Li|$LLZTO_xF_y$@PP|Li symmetrical cell consists of two pieces of $LLZTO_xF_y$@PP, with the $LLZTO_xF_y$ side facing the Li anode. 30 μL electrolyte was then added to the cell.

The assembly of the Li|$LLZTO_xF_y$@PP|LCO LMBs consists of one piece of $LLZTO_xF_y$@PP, with the $LLZTO_xF_y$ side facing the Li anode. 60 μL electrolyte was then added to the cell.

2. Electrochemical measurements

The Li||Li symmetric cell were prepared and polarized at a certain voltage (ΔV = 10 mV) for 3600 s to test the t_{Li+}. Formula are as follows:

$$t_+ = \frac{I_s(\Delta V - I_0 R_{el}^0)}{I_0(\Delta V - I_s R_{el}^s)}$$

R_0 and R_s are the initial and steady-state interface impedances, I_0 and I_s are the initial and steady-state currents in the chronoamperometry method, and ΔV is the potential difference in the chronoamperometry method.

The Li||Li symmetric cell with/without $LLZTO_{0.95}F_{0.05}$@PP using spectroelectrochemical cell were assembling for in-situ ATR-FTIR. Galvanostatic charges were performed using the LAND CT2001A at room temperature. The spectral resolution was 2 cm^{-1} and the scan velocity was 7.5 kHz. Each spectrum was measured by superimposing 32 interferograms.

The in-situ DRT were calculated from the electrochemical impedance spectroscopy data obtained by an electrochemical station (VMP3, BioLogic Science Instruments) from 7 MHz to 100 mHz. The Li||Li symmetric cell were prepared and polarized at a certain voltage (ΔV = 10 mV) for 3600 s to test the t_{Li+}. The linear sweep voltammetry curves were measured at a scan rate of 0.1 mV s^{-1}~1.0 mV s^{-1} by using VMP3.

The cyclic voltammogram curves of the Li||LCO cells between the potential ranges 3.0-4.6 V (V vs. Li/Li^+) at 30 °C. The galvanostatic charge/discharge performance of the Li||LCO cells between the potential ranges 3.0-4.6 V (V vs. Li/Li^+) at 30 °C was examined by battery tester (LAND CT2001A).

Ion diffusion experimentation: on one side of the H-cell, a methyl blue ethanol solution was added, while the other side contained pure ethanol solution. Two different types of separators were mounted between the two compartments. Since methyl blue ionizes in ethanol solution, dissociating into Na^+ and chromophore-

containing anions, the solution exhibits a blue color. By comparing the color changes in the H-cell over time, the diffusion of anions was evaluated, thereby simulating the diffusion behavior of anions in organic electrolytes.

3. Calculation method

Our spin-polarized density functional theory (DFT) calculations were carried out in the Vienna ab initio simulation package (VASP) based on the plane-wave basis sets with the projector augmented-wave metho. The exchange-correlation potential was treated by using a generalized gradient approximation (GGA) with the Perdew-Burke-Ernzerhof (PBE) parametrization. Meanwhile, a vacuum region of about 15 Å was applied to avoid the interaction between adjacent images. The energy cutoff was set to be 450 eV. The Brillouin-zone integration was sampled with a Γ-centered Monkhorst-Pack mesh of 1 × 1 × 1. The structures were fully relaxed until the maximum force on each atom was less than 0.03 eV $Å^{-1}$, and the energy convergent standard was 10^{-5} eV.

The adsorption energy Eads can be defined as, Eads = E*M - E* - EM, where E*M stands for the energy of the monolayer with the adsorbed M molecule, E* is the energy of surface, and EM is the energy of a M molecule under vacuum.

AIMD simulations used a C-point Brillouin zone for all interfacial supercell models. The DFT-D3 method was used to correct vander Waals forces. VESTA enables the visualization of all structures in a VASP calculation.

4. Materials characterization

Fourier-transform infrared spectroscopy (FTIR, Bruker INVENIO-R) was used to detect the functional groups. The crystal structure was determined by X-ray diffraction (XRD, Empyrean). X-ray photoelectron spectroscopy (XPS, ESCALAB

Xi+) was used to detect the change of chemical bonds. Morphology and micro-structure of $LLZTO_xF_y$ DES was characterized by SEM (LYRA3 GMU) and TEM (Talos F200X G2). Elements composition of $LLZTO_xF_y$ DES separator had been qualitatively analyzed by scanning electron microscope EDS spectrometer. The Time of Flight Secondary Ion Mass Spectrometry (TOF-SIMS) was characterized on the TESCAN LYRA3 GMU.

Supplementary Figure

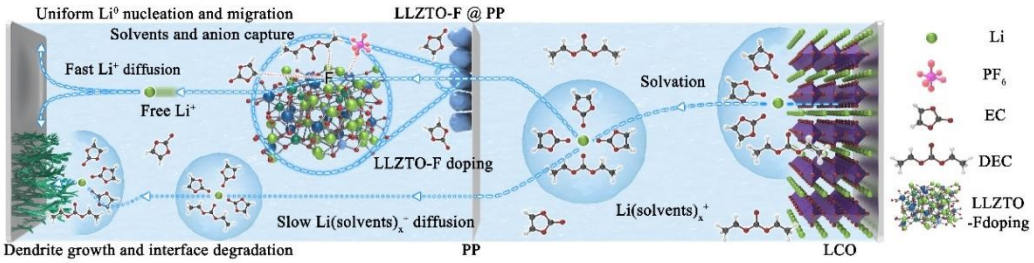

Fig. S1 Schematic of LLZTO-F DES ion kinetic promoter as the functional PP separator modification layer of LMBs for the regulation of the desolvation of $Li(solvents)_x^+$.

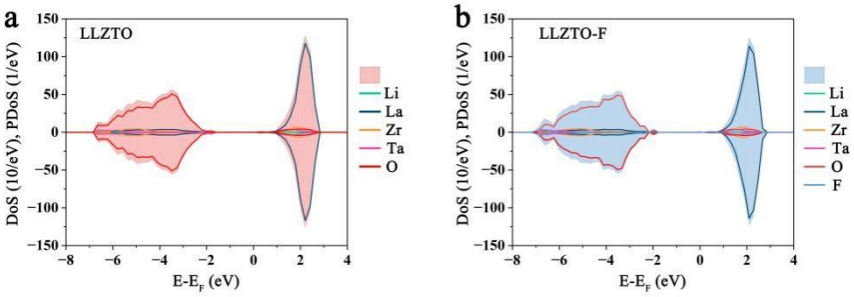

Fig. S2 Partial density of states of (a) LLZTO and (b) LLZTO-F.

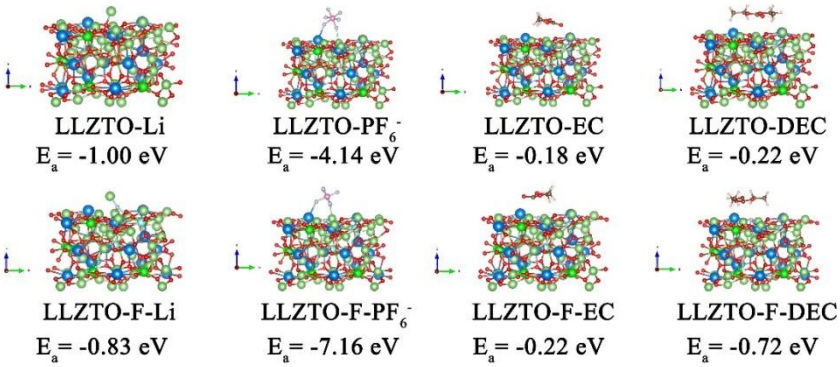

Fig. S3 The models for Li^+, anions, and solvents on the LLZTO and LLZTO-F.

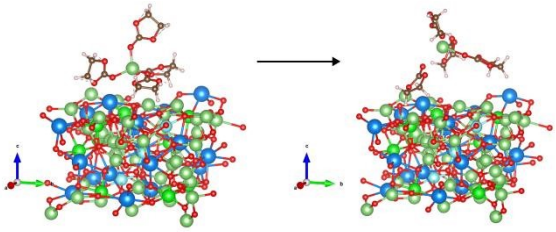

Fig. S4 Desolvation process of $Li(EC)_4^+$ on the LLZTO.

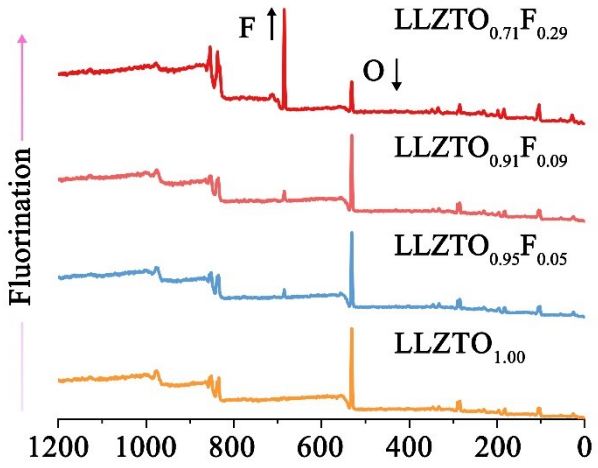

Fig. S5 The comparisons of XPS spectra of $LLZTO_xF_y$.

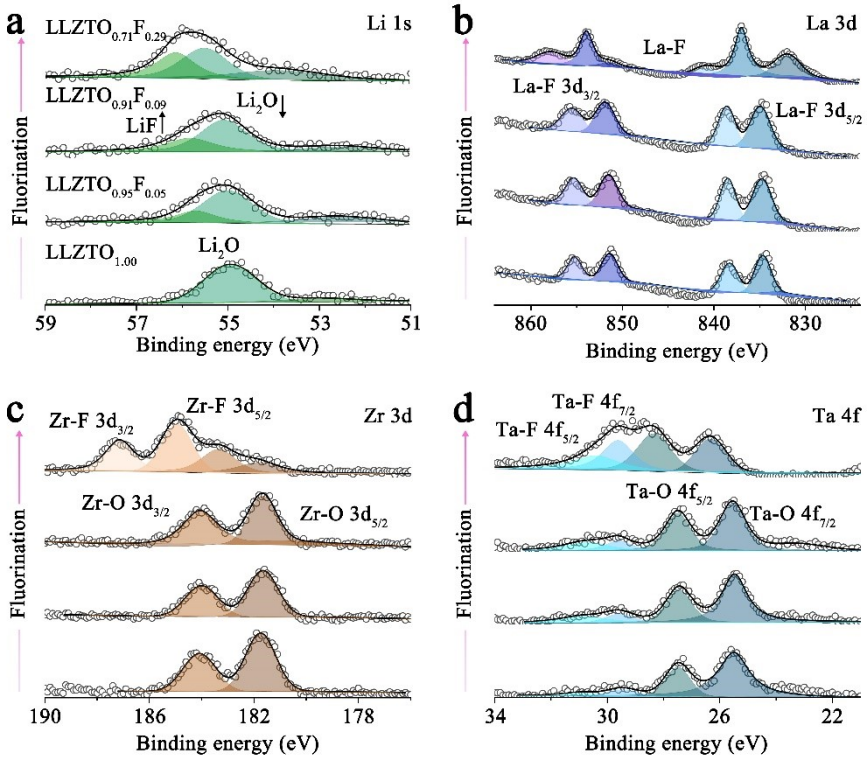

Fig. S6 The comparisons of Li 1s, La 3d, Zr 3d, and Ta 4f of $LLZTO_xF_y$.

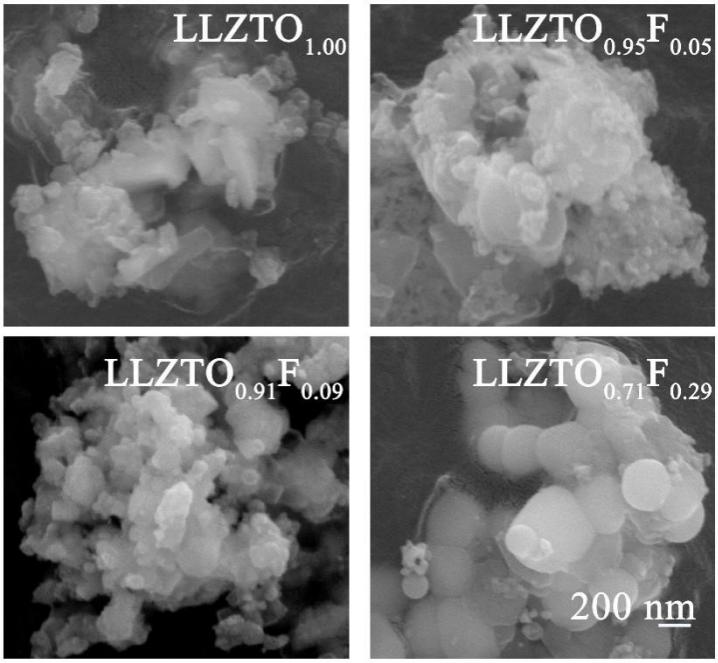

Fig. S7 SEM images of $LLZTO_xF_y$.

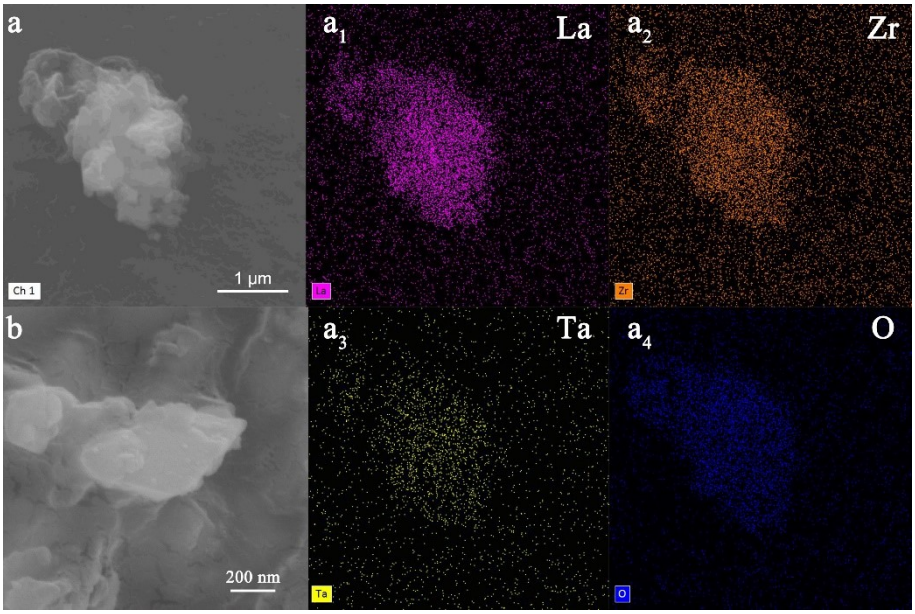

Fig. S8 SEM and mappings images of $LLZTO_{1.00}$.

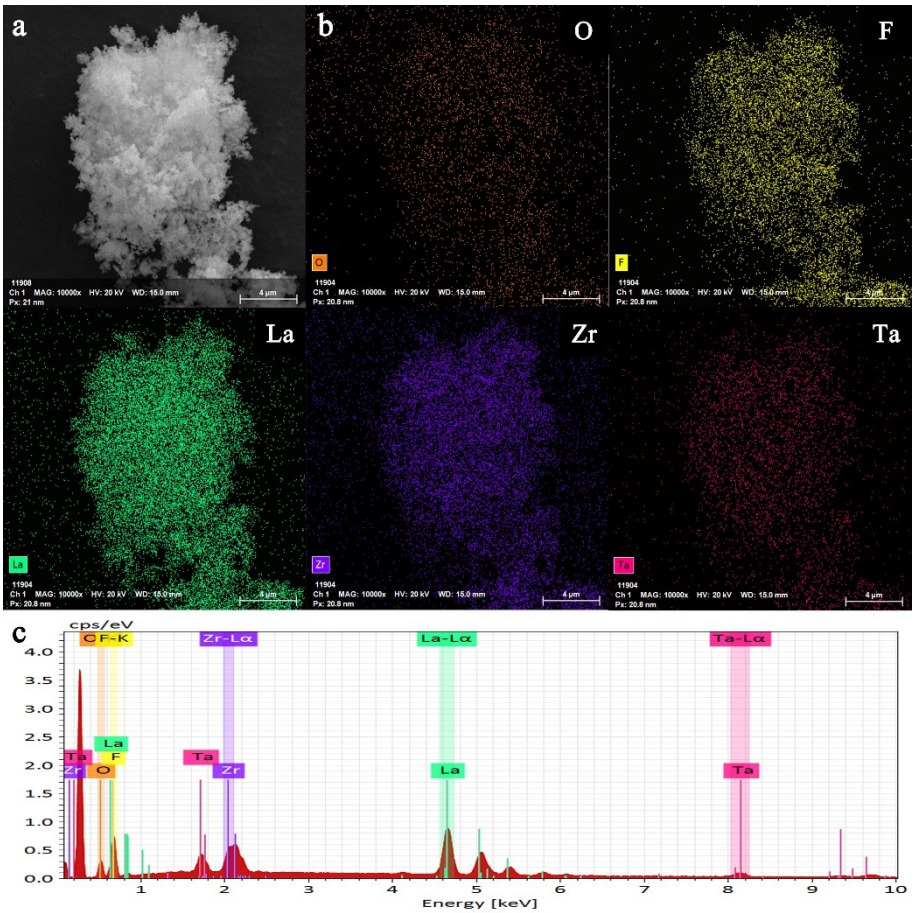

Fig. S9 (a) SEM image, (b-c) corresponding EDX elemental mappings of $LLZTO_{0.95}F_{0.05}$.

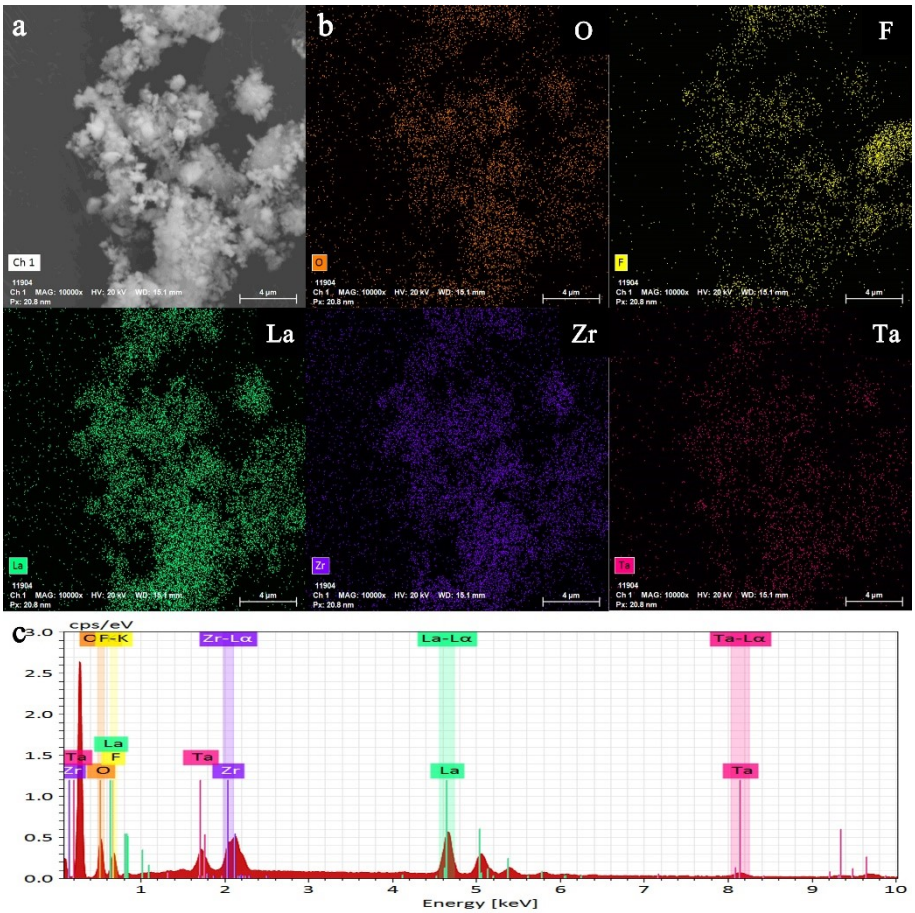

Fig. S10 (a) SEM image, (b-c) corresponding EDX elemental mappings of $LLZTO_{0.91}F_{0.09}$.

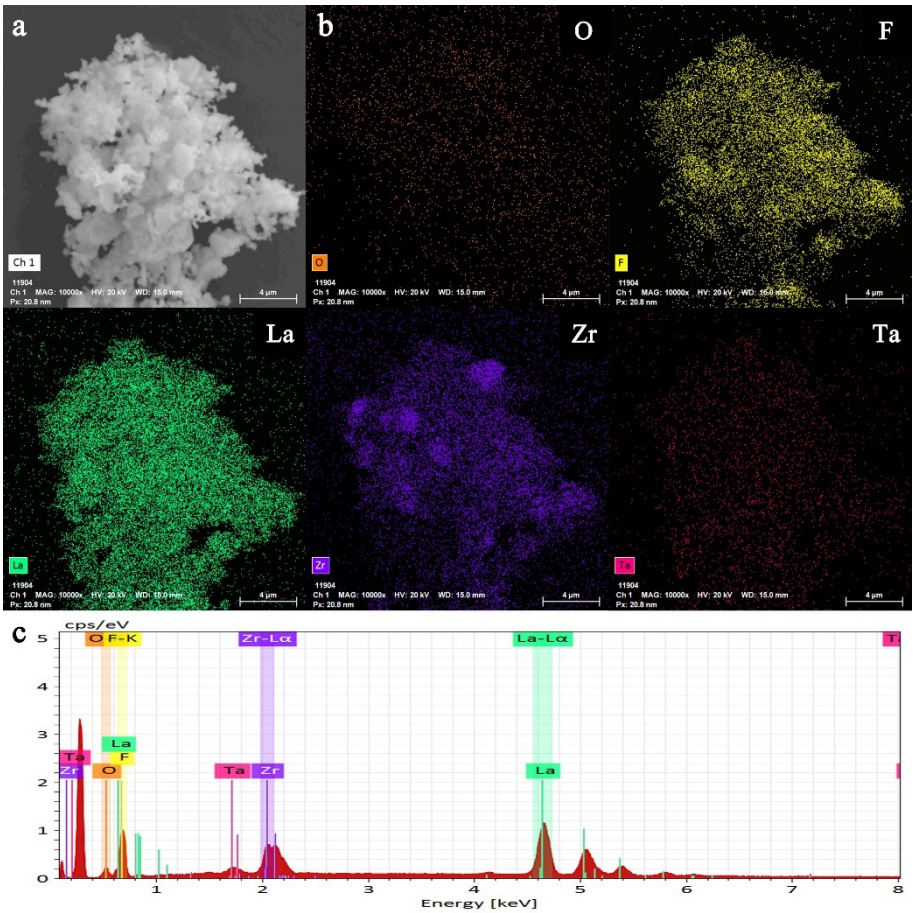

Fig. S11 (a) SEM image, (b-c) corresponding EDX elemental mappings of $LLZTO_{0.71}F_{0.29}$.

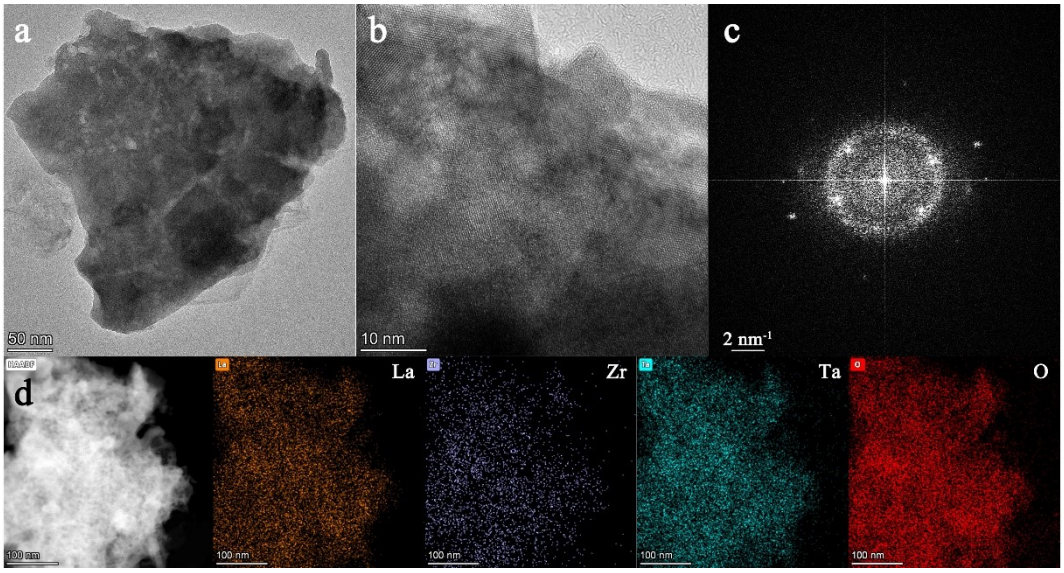

Fig. S12 (a-b) HRTEM images, (c) diffraction rings and (d) corresponding EDX elemental mappings of $LLZTO_{1.00}$.

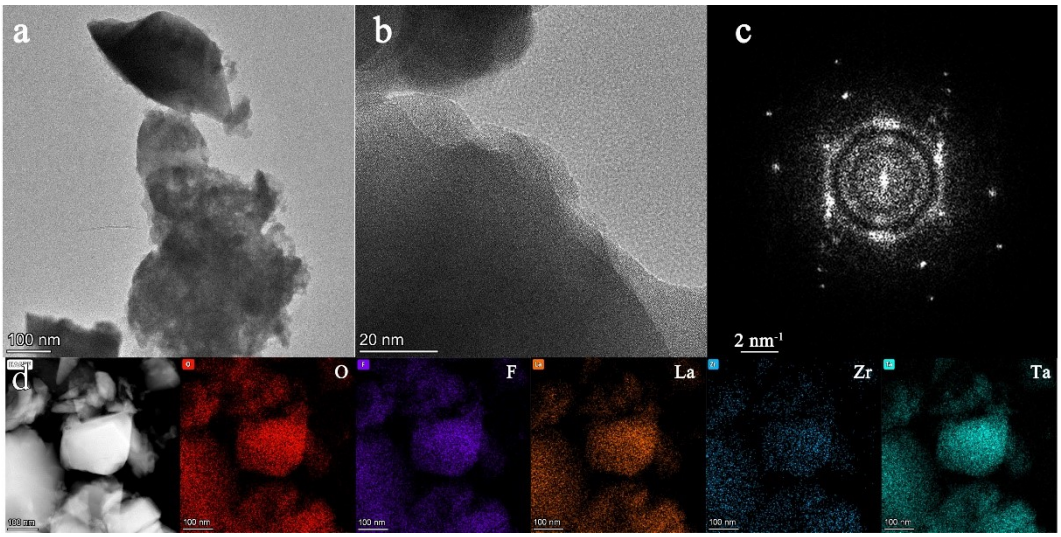

Fig. S13 (a-b) HRTEM images, (c) diffraction rings and (d) corresponding EDX elemental mappings of $LLZTO_{0.91}F_{0.09}$.

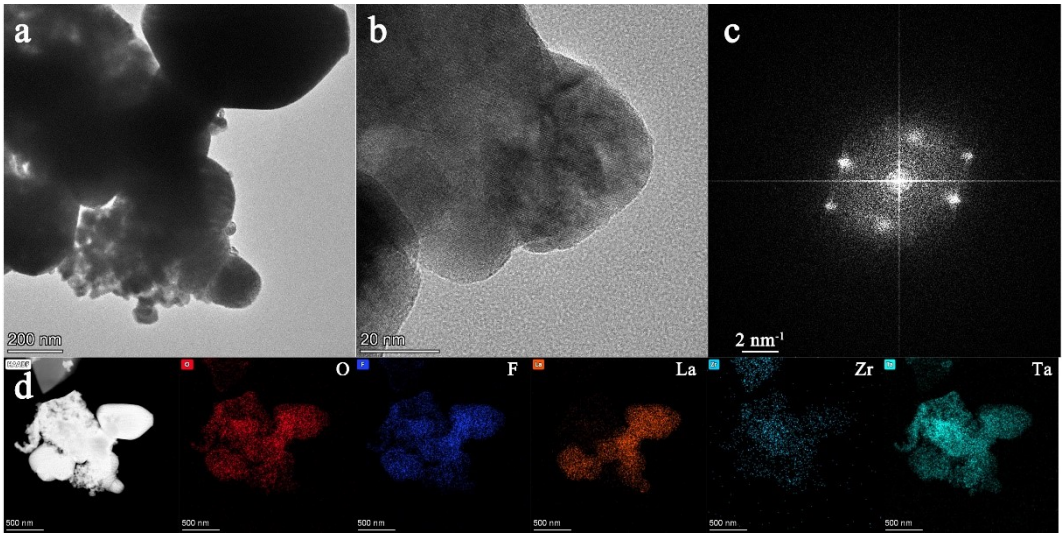

Fig. S14 (a-b) HRTEM images, (c) diffraction rings and (d) corresponding EDX elemental mappings of $LLZTO_{0.71}F_{0.29}$.

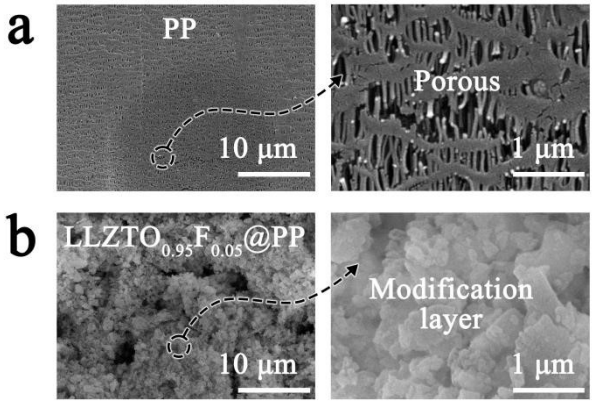

Fig. S15 SEM images of (a) PP and (b) $LLZTO_{0.95}F_{0.09}$@PP.

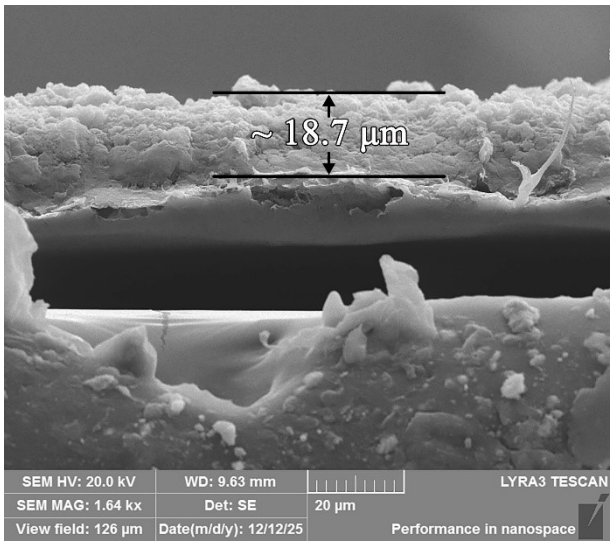

Fig. S16 SEM images of cross-section of $LLZTO_{0.95}F_{0.09}$@PP.

Fig. S17 Contact angle measurements with electrolyte for PP and $LLZTO_{0.95}F_{0.05}$@PP.

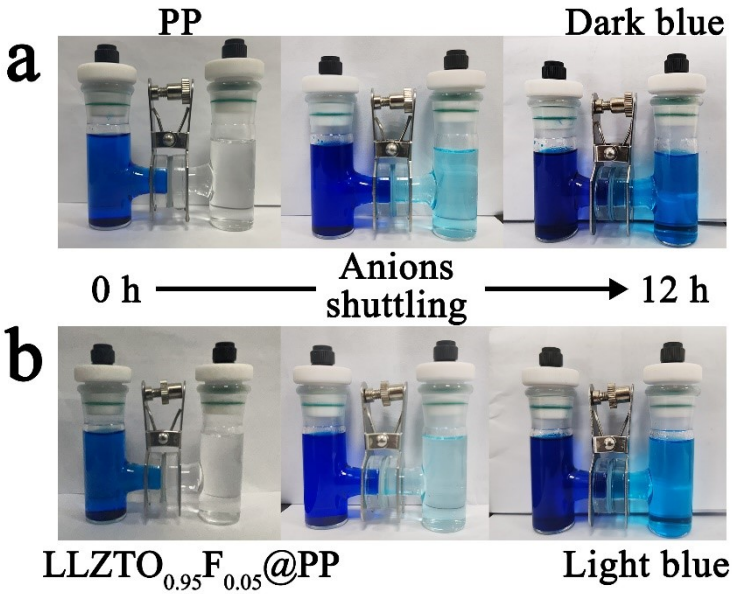

Fig. S18 The anion shuttling experiments of PP and $LLZTO_{0.95}F_{0.05}$@PP. In H-type cell, the left side is methyl blue/ethanol solution and the right side is ethanol solution.

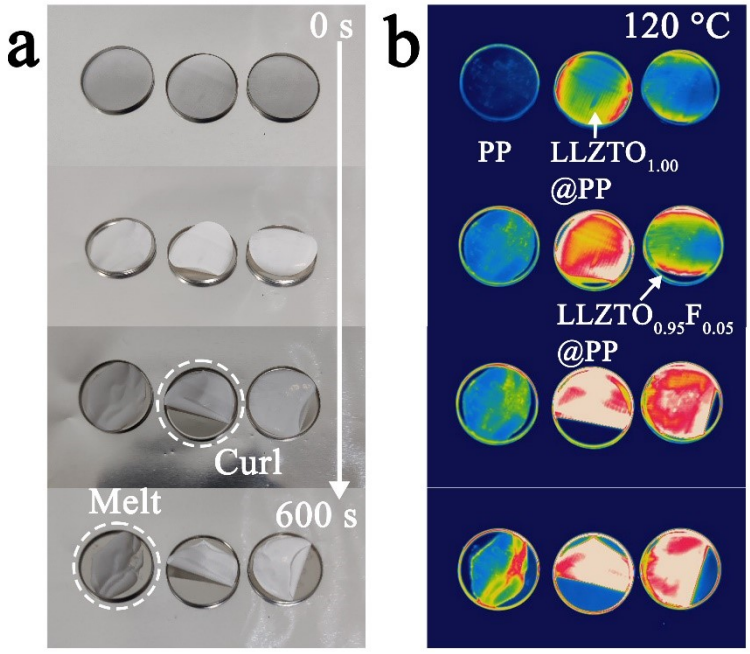

Fig. S19 (a) Thermal stability tests and (b) corresponding infrared thermal images.

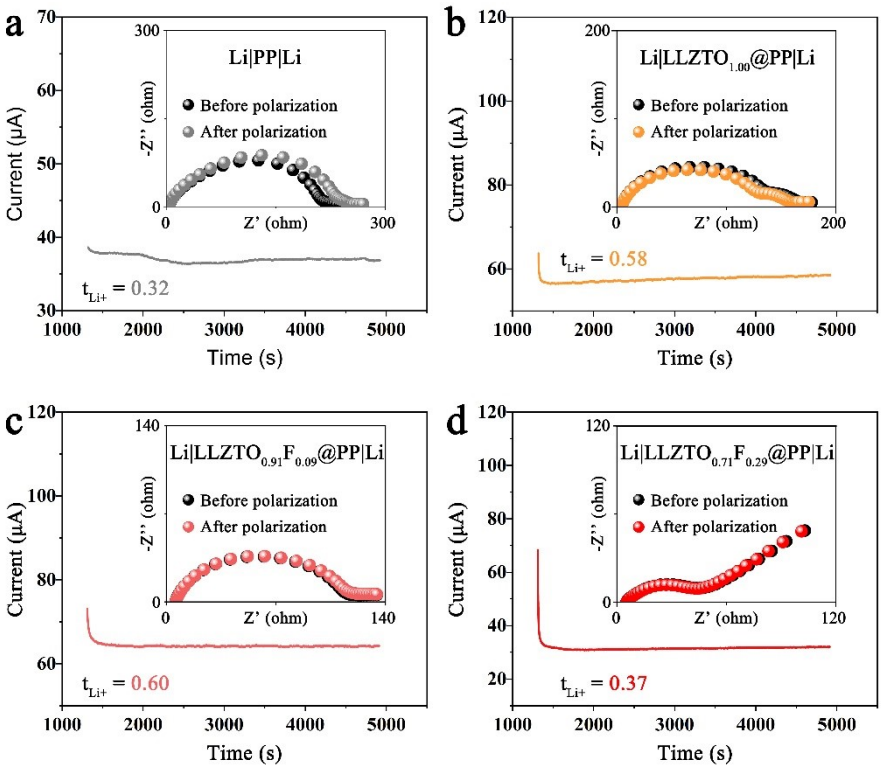

Fig. S20 Polarization curve with a perturbation of 10 mV of Li||Li symmetric cells (Insert: electrochemical impedance spectroscopy analysis before and after polarization of symmetric cell.

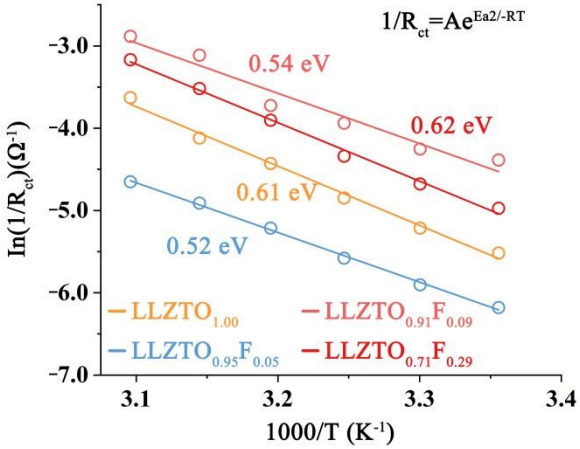

Fig. S21 Activation energy of $LLZTO_xF_y$@PP-based Li||Li symmetric cells.

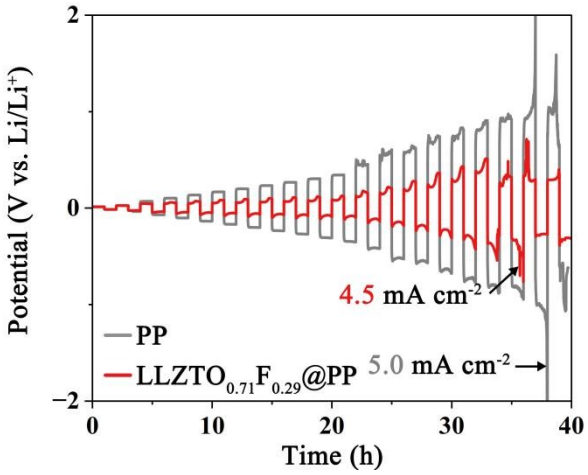

Fig. S22 Critical current density values of Li||Li symmetric cells with PP and $LLZTO_{0.71}F_{0.29}$@PP.

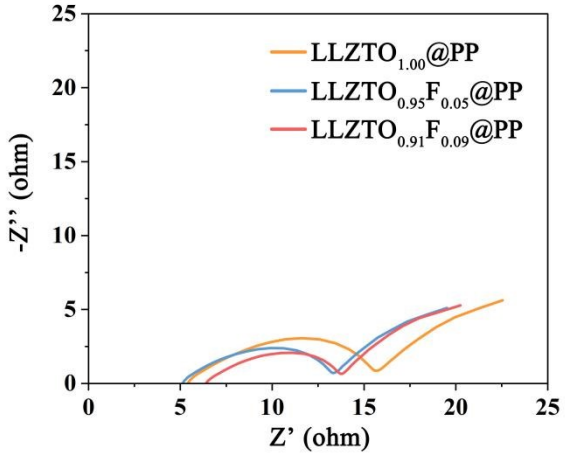

Fig. S23 EIS of Li||Li symmetric cells after rate test.

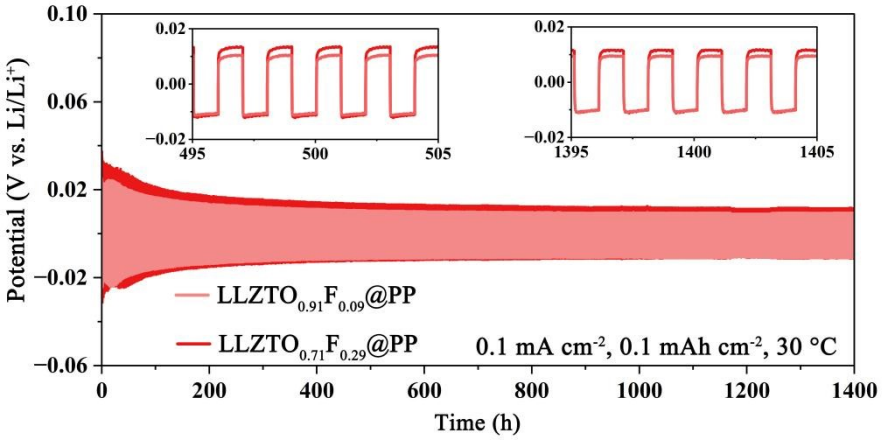

Fig. S24 Galvanostatic voltage profiles of Li||Li symmetric cell at 0.1 mA cm^{-2},

0.1 mAh cm^{-2}.

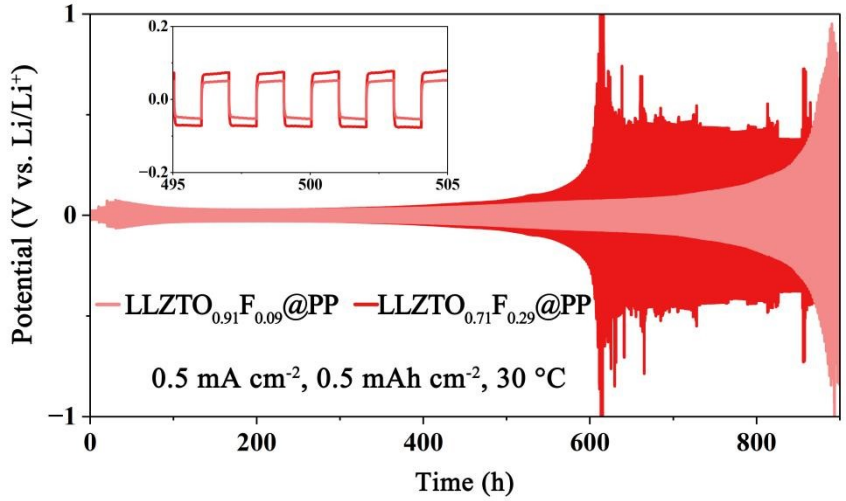

Fig. S25 Galvanostatic voltage profiles of Li||Li symmetric cell at 0.5 mA cm^{-2}, 0.5 mAh cm^{-2}.

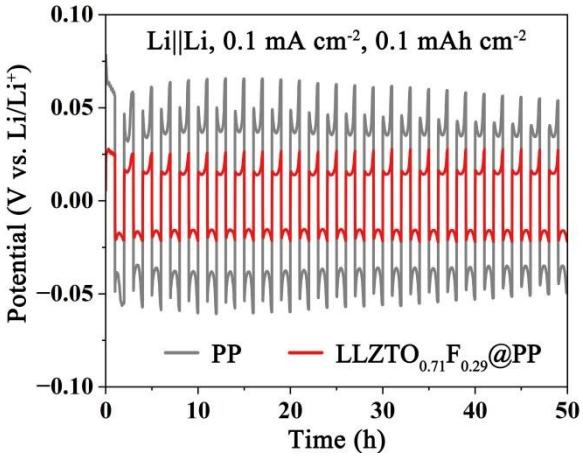

Fig. S26 Galvanostatic voltage profiles of Li|PP|Li and Li|LLZTO$_{0.71}$F$_{0.29}$@PP|Li symmetric cell at 0.1 mA cm^{-2}, 0.1 mAh cm^{-2}.

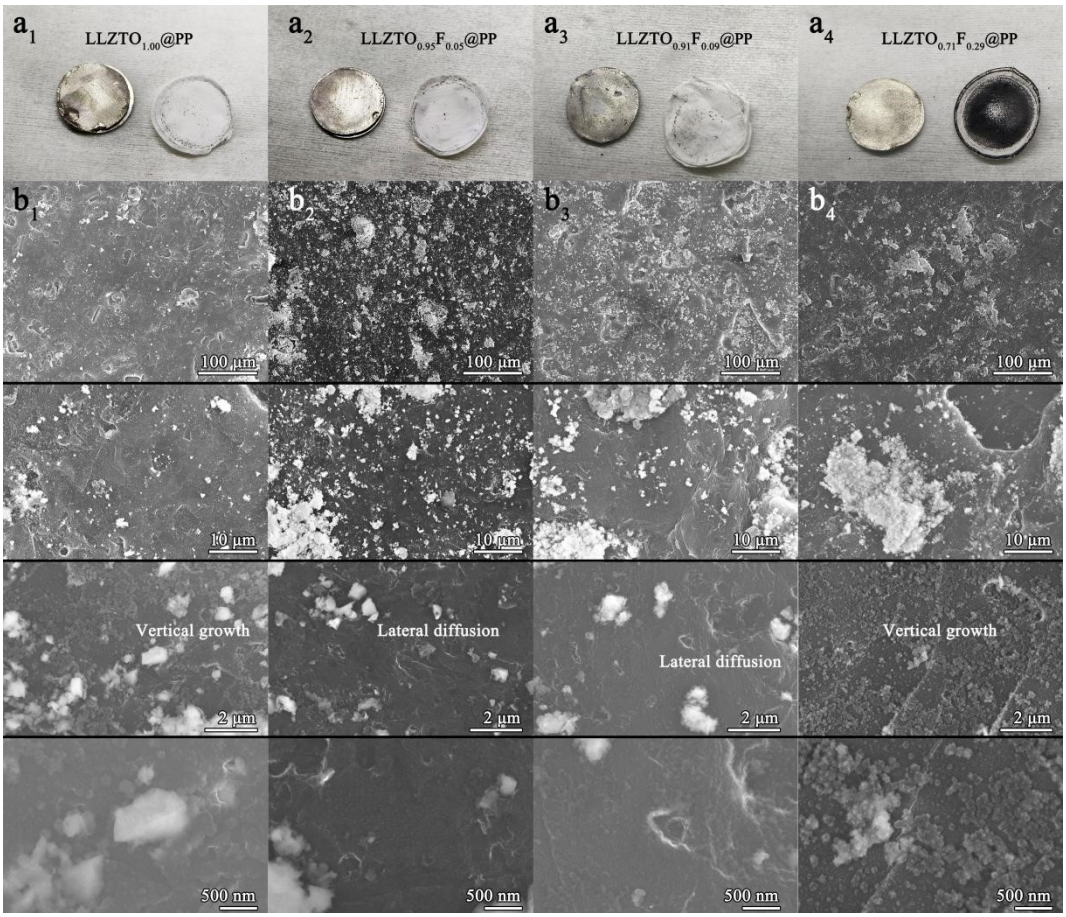

Fig. S27 (a) Digital pictures and (b) SEM images of Li and $LLZTO_xF_y$@PP after cycling.

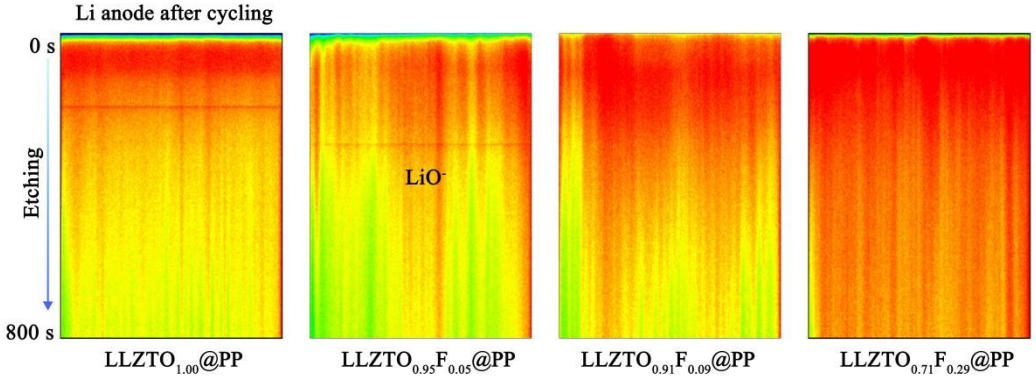

Fig. S28 The TOF-SIMS sputtered volumes of Li anode after cycling.

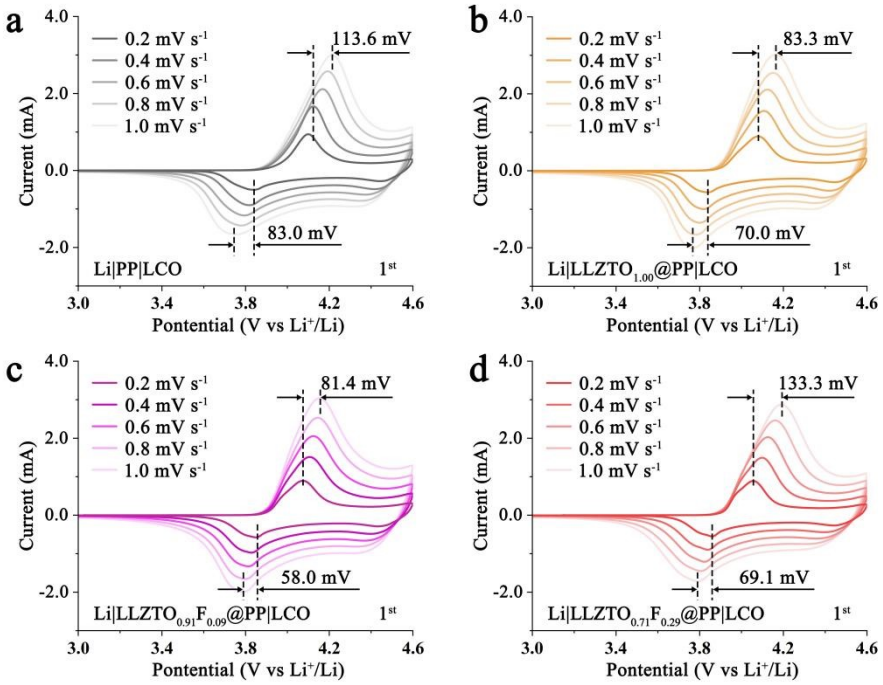

Fig. S29 Cyclic voltammogram of Li|LLZTO$_x$F$_y$@PP|LCO in the operating voltage window of 3.0-4.6 V, from 0.2 mV s^{-1} to 1.0 mV s^{-1}.

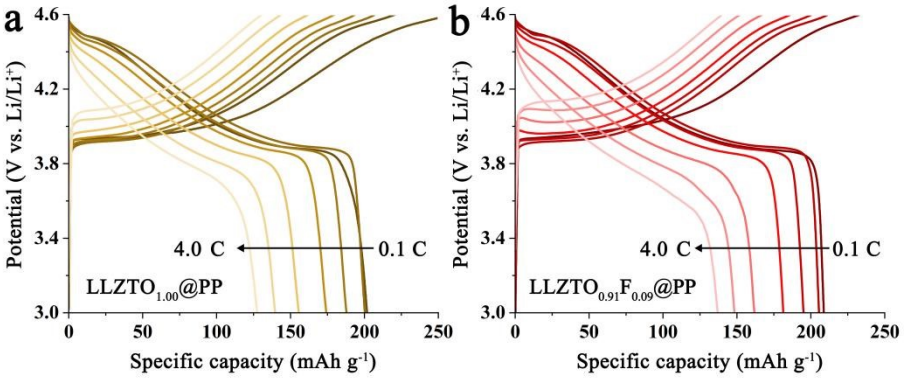

Fig. S30 Charge-discharge curves of the cells with LLZTO$_{1.00}$@PP and LLZTO$_{0.91}$F$_{0.09}$@PP.

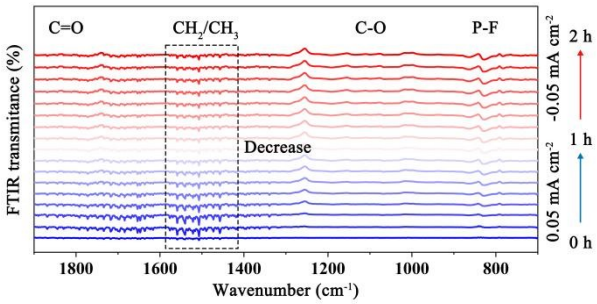

Fig. S31 In-situ FTIR spectroscopy reveals the solvation structure evolution of $Li(solvent)_x^+$ in $LLZTO_{1.00}$@PP based Li||Li symmetric cells.

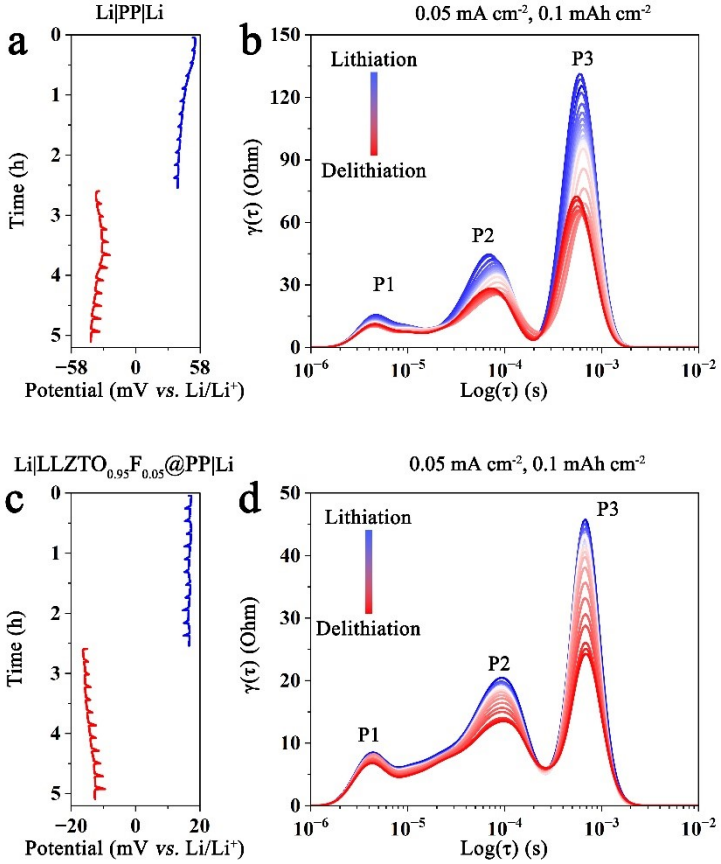

Fig. S32 (a) Voltage profiles and (b) DRT of Li|PP|Li symmetric cell under 0.05 mA cm^{-2}, 0.05 mAh cm^{-2}. (c) Voltage profiles and (d) DRT of $Li|LLZTO_{0.95}F_{0.05}$@PP|Li symmetric cell under 0.05 mA cm^{-2}, 0.05 mAh cm^{-2}.